Evolutionary Design Principles of a Bacterial Signalling Network

Markus Kollmann,[1,*] Kilian Bartholome,[1]
Linda Løvdok,[2] Jens Timmer,[1] and Victor Sourjik[2]

[1] *Universität Freiburg, Institut für Physik, 79104 Freiburg, Germany*
[2] *Zentrum für Molekulare Biologie Heidelberg, 69120 Heidelberg, Germany*

Abstract

Cellular biochemical networks have to function in a noisy environment using imperfect components. Especially networks involved in gene regulation or signal transduction allow only for small output tolerances and the underlying network structures can be expected to have evolved for inherent robustness against perturbations [1]. Here, we combine theoretical and experimental analysis to investigate an optimal design for the signalling network of bacterial chemotaxis, one of the most thoroughly studied signalling networks in biology. We experimentally identify intercellular variations in expression levels of chemotaxis proteins as the main source of perturbations and use computer simulations to quantify the robustness of several hypothetical chemotaxis pathway topologies to such gene expression noise. We demonstrate that the experimentally established topology of the chemotaxis network in *Escherichia coli* is one of the smallest sufficiently robust structures, allowing accurate chemotactic response for almost all individuals within a population. Our results suggest that this pathway has evolved to show an optimal chemotactic performance while minimising the cost of resources associated with high levels of protein expression. Moreover, the underlying topological design principles compensating for intercellular variations seem to be universal among all known or predicted bacterial chemosensory systems [2].

*Corresponding author:markus.kollmann@fdm.uni-freiburg.de

Errors in signal transduction can lead to wrong development and behavioural decisions, and result in growth impairment or, in multicellular organisms, to cancer [1]. Therefore one expects a strong selective pressure towards networks showing intrinsic robustness against the various sources of inter- and intra-cellular perturbations, such as fluctuations in protein concentration. Due to limitations in our quantitative understanding of most signalling networks, only few detailed studies of network robustness are currently available [3–6]. One of the best-studied simple signalling systems is bacterial chemotaxis, which allows bacteria to navigate in gradients of chemical attractants or repellents. Here, information about ambient changes in chemo-ligand are transmitted from receptors on the cell surface to the flagellar motors by a stimulation-dependent phosphorylation of a diffusible response regulator protein CheY. Most biochemical rate constants and average concentrations of chemotaxis proteins under standard conditions have been determined [7], making chemotaxis an excellent system for a quantitative analysis. Another advantage of the chemotaxis pathway is its relative isolation from other cellular processes, such as metabolism, which allows treating the pathway as an independent module [8]. In the following we analyse design principles of the chemotaxis pathway from an evolutionary perspective.

Chemotaxis pathways can sense relative changes of attractant concentrations as small as two percent over a dynamic concentration range of five orders of magnitude [9]. Previous quantitative analysis showed that such a large dynamic range can be explained by a combination of allosteric signal amplification by receptor clusters [10, 11] and a precise adaptation mechanism ([3, 12–14]). Precise adaptation is the ability to return to the same level of pathway activity under conditions of continuous stimulation. Failure of this systems property would lead to permanent swimming or tumbling behaviour and thus to the loss of chemotactic ability. In *E. coli*, sudden addition of attractant leads to an almost instantaneous decline in receptor activity followed by the slow adaptation process. The most simple topology of a chemotactic signalling network which allows for precise adaptation is a two-state model proposed by Barkai & Leibler (BL model) [3]. Their model is schematically drawn in Fig. 1a. The core property of the model is that receptors sensing chemo-ligands can be reversibly methylated. A higher level of methylation increases the probability of a receptor to switch to an active state. Almost perfect adaptation results from a constantly working methyltransferase (CheR) balanced by a methylesterase (CheB), which works only

on active receptors [15]. Active receptors enhance autophosphorylation activity of CheA, which in turn phosphorylates CheY.

The BL model can readily explain the robustness of precise adaptation against a wide range of variations in kinetic parameters and protein concentrations as a consequence of integral feedback control at the methylation level [3]. However, the quantity under evolutionary selection is the stationary level of pathway activity, e.g. the concentration of phosphorylated CheY, which is not robust to such large variations [4]. It is possible to construct other but larger adaptive topologies having equal input-output characteristic, Figs. 1b-1d. The larger topologies are not necessarily more robust against perturbations as there exists a trade-off between the gain in degrees of freedom to design better networks and the increasing amount of components, which are subject to intercellular variations.

There are multiple sources of such variations, both intracellular and intercellular. The intracellular variations can arise from stochastic fluctuations of local protein concentrations within the cell. Although it has been found experimentally that low concentration of CheR induce fluctuations in the network output on a 100s time scale, they are most likely too short to show a significant negative effect on the fitness [16]. Spatial variations effecting co-localisation of reaction partners scale with the size distribution of the individuals and should therefore be moderate [17]. Thus, the dominating source of perturbations in a bacterial cell population is intercellular variation of protein concentrations arising from protein synthesis and decay [18]. Such variations can persist on the generation time scale since there is no evidence for an active degradation of chemotaxis proteins under standard growth and assay conditions and the decrease in protein levels mainly results from dilution during cell division. Robustness against variations in protein concentrations should therefore be subject to evolutionary selection.

To measure experimentally the amplitude of such intercellular variations in the levels of chemotaxis proteins, we replaced a native *cheY* gene in *E. coli* with *cheY* fused to a yellow fluorescent protein (*cheY-eyfp*) as a translational reporter. The reporter construct is thus expressed from the native promoter as part of polycistronic mRNA of the *meche* operon that also encodes Tar and Tap chemoreceptors, and the cytosolic proteins CheR, CheB, CheY, and CheZ. The proteins CheA and CheW are expressed as part of another, the *mocha*, operon. Expression of both chemotaxis operons and that of another major receptor Tsr is negatively controlled by an anti-sigma factor FlgM [19, 20]. The protein levels in

the population (Fig. 2a) show large intercellular variation with an apparently asymmetric distribution (see Ref. [21]). The *gene expression noise*, $\eta = \sigma/n$, where σ is the standard deviation and n is the mean expression, depends on the level of gene transcription, as shown by deleting the upstream transcription inhibitor, the anti-sigma factor FlgM (Fig. 2a). Such decrease in the gene expression noise with the level of transcription appears to be general, since it was also observed for several artificial promoters (see Supplementary Information). Recently, model-based analysis showed that transcription should dominate gene expression noise between proteins when expressed from the same mRNA transcript [22, 23]. We confirmed this conclusion by comparing the variation in the levels of CheY and CheZ expressed as fusions to yellow and cyan fluorescent proteins, YFP and CFP, from the same promoter in the same order as they are positioned on the chromosome and under their native ribosome-binding sequences. There is a strong co-variation in the expression levels of both, defined as extrinsic noise η_{ex}, which arises mainly from fluctuations in transcriptional activity, and only a moderate independent variation, defined as intrinsic noise η_{in}, as a consequence of stochastic effects in translation (Ref. [18] and Fig. 2b). Intrinsic and extrinsic noise are related to the total gene expression noise by $\eta^2 = \eta_{in}^2 + \eta_{ex}^2$. Proteins expressed from two different chemotaxis operons, *mocha* and *meche*, which belong to the same regulon, also show significant co-variation in gene expression noise (Fig. 2b, inset) but with a 25 percent increase of intrinsic noise in comparison with proteins expressed from the same operon (Fig. 2b, main panel).

We further experimentally determined the effect of co-variation in the levels of all signalling proteins on chemotactic behaviour (Fig. 3). Concerted overexpression of all proteins up to 6.6-fold above the native level had little effect on the chemotaxis efficiency, as measured by a chemotaxis-driven spreading of bacteria in an attractant gradient created by nutrient depletion in soft agar (swarm assay). Thus, CheY-P concentration in the overexpressing cells must be in the working range of a flagellar motor (see below), and cell swimming pattern was indeed similar to that of the wild type (data not shown). In addition, we used an in-vivo assay based on fluorescence resonance energy transfer (FRET) [9] to show that the kinase activity is elevated 2.1-fold upon a 6.6-fold overexpression of all chemotaxis proteins except for CheY and CheZ. The assay measures the intracellular concentration of the CheYp-CheZ complex, for CheY and CheZ expressed as fusions to yellow and cyan fluorescent proteins, YFP and CFP, respectively (see Methods). Relying on these experimental data, we anal-

ysed mathematically the robustness of the four network topologies drawn in Fig. 1 under conditions of natural perturbations.

In adapted cells, the level of CheYp can vary only about one third from its optimal value, since outside this concentration regime the cell either tumbles or swims continuously and cannot properly respond to stimuli [24]. The chemotatic efficiency of a population therefore depends on the fraction of bacteria whose CheYp levels are within these limits. In the computer simulations (see Methods), we used the experimentally determined gene expression noise (Fig. 2) as an estimate for the minimum intercellular variations for the proteins encoded by the *meche* operon. We tested the different hypothetical network topologies, shown in Fig. 1, for their ability to reproduce the chemotaxis efficiency from swarming experiments for concerted variations of mean expression levels, Fig. 3. The *E. coli* topology (Fig. 1c) reproduces accurately the experimental data, whereas simpler topologies (e.g. Fig. 1a) fail to match the data. To further quantify the robustness of the different network topologies, we calculated the fraction of bacteria showing chemotactic response for different strength of gene expression noise (Fig. 4). The topologies Fig. 1c and Fig. 1d allow for the highest fraction of cells in the population to respond accurately to changes in chemo-ligand concentrations. As we have not included all sources of intercellular variations, these results can be seen as an upper bound of the chemotactic efficiency for a population. The topologies Fig. 1b, 1c, and 1d are sufficiently robust to compensate for strong transcriptional noise (Fig. 4a) but tolerate only a moderate increase in intrinsic noise (Fig. 4b).

There are two key features accounting for the higher robustness of the topologies shown in Fig. 1c, 1d. First, robustness against extrinsic noise requires a balance of phosphatase and kinase reactions and similar requirements for the methylation process, as shown by mathematical analysis in Box 1. The conditions for a robust adaptive chemotaxis pathway is that CheYp demands a phosphatase (CheZ) while CheBp must not have one. Also the methyltransferase, CheR, has to work at saturation. But from our theoretical analysis and swarming experiments we can see that this kind of robustness is only valid for concentrations larger than the wild-type level (Fig. 3a). The strong decrease in the number of chemotactic bacteria at lower expression levels (Fig. 3a inset) arises because the total CheY concentration approaches the optimal CheYp value (midpoint of the motor response curve) and thus violates the homogeneity condition as explained in Box 1. Consequently, the bacterium switches to permanent swimming behaviour and cannot show a chemotactic response. The

increase in chemotatic performance of the topologies Fig. 1b and 1c with the mean expression level can be explained by an accompanying decline of the gene expression noise (Fig. 2a, and Ref. [18]) and a significantly higher concentration of CheY than the adapted level CheYp. The location of the wild-type concentration as shown in Fig. 3a seems to reflect a selective pressure towards overall low protein concentrations. Such pressure can be explained by a negative effect of high protein expression on cell growth, and the growth rate of *flgM* strain in liquid culture was indeed only 0.83 ± 0.03 of the wild type.

The second topological feature leading to higher swarming efficiency is the CheB phosphorylation resulting in an additional negative feedback loop (Fig. 1c, 1d). As shown in Box 2, this second feedback loop compensates partially for deviations from the optimal CheYp level, e.g. due to intrinsic noise, without changing the input-output characteristics. The two design principles described above increase the robustness of the network (Fig. 1c, 1d) against intercellular noise and thus lead to an on average higher fitness of the individuals. Moreover, the essential features for these design principles seem to be present among all predicted pathway topologies of bacterial chemotaxis which employ receptor methylation for adaption [2]. In particular, the CheB phosphorylation feedback is universal in all bacteria with known chemotaxis systems and although many bacteria lack CheZ, the function of CheY phophatase is taken over by another protein of by kinase itself.

To complete our picture for the components involved in the chemotaxis pathway, it can be further shown for our model that: (i) a methyltransferase (CheR) has to exist, because auto-methylation of inactive receptors violates robustness against extrinsic noise (see Box 1 and Supplementary Information) although it satisfies the conditions for precise adaptation [15], (ii) a negative feedback loop, resulting from inactivation of CheR by phophotransfer from CheA, shows only about half the efficiency for noise compensation of a feedback via CheB phosphorylation as a consequence of CheR working at saturation and (iii) additional feedback loops , as introduced in Fig. 1d by dashed lines, do not give significant improvement of the chemotaxis efficiency (Fig. 4).

Considering their short generation time and strong competition for the available nutrients in their natural environments, bacteria are one of the best systems to analyse optimal design from an evolutionary perspective [14]. Reflecting strong selection, the chemotaxis pathway in *E. coli* appears to be optimised for high sensitivity, fast response, and perfect adaptation [12–14]. Therefore, one expects also the network structure to be the outcome of

an evolutionary optimisation process in order to increase chemotatic efficiency. And indeed, as shown in this work, the experimentally established design of the chemotaxis network in *E. coli* is a minimal topology providing high robustness to physiological perturbations. This network design can compensate for strong co-variations in gene expression but the negative effect of uncorrelated variations on the chemotaxis efficiency can only be attenuated. Thus, one reason for the organisation of bacterial genes into operons and regulons might be to minimise these uncorrelated variations in gene expression [23]. Similar correlations in gene expression noise, as shown in Fig. 2a, have been recently found also in eukaryotes for genes under identical control [25, 26]. We can therefore expect that analog design principles, compensating for intercellular variations, will apply to all signalling networks and gene regulation systems whenever precise regulation of an output signal to a given level is demanded.

Box 1. Robustness against Variations in Transcriptional Activity

A general deterministic description for the concentrations of the N different phosphorylation and methylation states $\mathbf{y}(t) = \{y_1(t), ..., y_N(t)\}$ of a signalling pathway are given by the equations

$$\partial_t y_i(t) = F_i(\mathbf{y}(t)|\mathbf{x}^T) \tag{1}$$

(see Supplementary Information for details). The sum over different states, $\{y_i\}_k$, of the protein with index k is connected to its total concentration by $\sum_{\{y_i\}_k} y_i(t) = x_k^T$. For the stationary solution, $F_i(\mathbf{y}(t)|\mathbf{x}^T) = 0$, to be invariant against co-varying total protein concentrations, e.g. due to a λ-fold change in transcriptional activity $\mathbf{x}^T = \{x_1^T(t), ..., x_M^T(t)\} \rightarrow \{\lambda x_1^T(t), ..., \lambda x_M^T(t)\}$ of the M chemotaxis proteins, we have to demand homogeneity of F with respect to $\mathbf{x}^T$,

$$F_i(\mathbf{y}(t)|\lambda\mathbf{x}^T) = \lambda^{\mu_i} F_i(\mathbf{y}(t)|\mathbf{x}^T) \tag{2}$$

with $\mu_i = \{1, 2, ..\}$. For the equations corresponding to the topologies Fig. 1a the homogeneity condition can not be satisfied. For topologies Fig. 1b, 1c, 1d we have the case $F_i(\mathbf{y}(t)|\lambda\mathbf{x}^T) \approx \lambda F_i(\mathbf{y}(t)|\mathbf{x}^T)$ for $\lambda > 1$ and therefore these topologies are invariant against changes in transcriptional activity of signalling proteins at expression levels higher than the wild type. This finding is confirmed by an over-expression experiment as shown in Fig. 3. Because the functions F_i are linear in λ, changes in transcriptional activity correspond to a rescaling of time $t \rightarrow \lambda t$. As a result, adaptation times do not change significantly with increasing λ, because the resulting faster reaction rates get partially compensated by the increased amount of proteins which have to be activated or deactivated.

As shown in the Supplementary Information, the topological consequences of invariance in λ for the chemotaxis pathway are: (i) the methyltransferase protein, CheR, *has to* work at saturation, (ii) a phosphatase for CheYp *must* exist, and (iii) if the methylesterase is active in phosphorylated form (CheBp), as it is the case for all known bacterial chemotaxis systems [2], it *must not* have a phosphatase. Other necessary conditions are to choose the kinetic constants for the phophotransfer such that the concentrations of CheAp and CheYp are significantly smaller than their inactive forms. Violation of latter condition leads, e.g. to the decline of chemotatic efficiency for concentrations of CheY below the wild type level (Fig. 3a inset).

Box 2. Error Reduction Mechanisms

Errors in the output signal arising from independent variations of protein levels (intrinsic noise) and deviations from the optimal rate constants can be partially compensated by additional negative feedback loops (Fig. 1). In the following, we focus on the gain in robustness due to activation of the methylesterase, CheB, by phosphotransfer from CheA. To illustrate the point we simplify the *E. coli* chemotaxis topology (Fig. 1c) such that any receptor has only one methylation site and the activity of methylated receptors depend on the ambient chemo-ligand concentration. Non-methylated receptors remain inactive. Using Michaelis-Menten kinetics, the steady state equation for the methylation process reads

$$\partial_t T_M = k_R R - k_B Bp \, \frac{T_A}{K_B + T_A} = 0 \quad , \tag{3}$$

with k_R and k_B the associated rate constants and K_B the Michaelis-Menten constant for binding of CheBp to the receptors complex (see Ref. [3]). The concentrations of methylated and active receptors are denoted by T_M and T_A, respectively. For the topologies Fig. 1c, 1d the methylesterase, $Bp = Bp(A)$, is active only in phosphorylated form and thus depends on the concentration of the phophodonor, CheAp, which is part of the receptor complex. We have also assumed that the methyltransferase, $R =$ [CheR], works at saturation and only active receptors can be demethylated. Similar steady state equations can be given for the phosphorylated protein concentrations $Bp =$ [CheBp], $Yp =$ [CheYp]. The stationary equation for $Ap =$ [CheAp] is given by

$$k_A \, T_A \, (A^T - Ap) - k_Y \, Ap \, (Y^T - Yp) = 0 \tag{4}$$

with $Yp = k_Y Ap \, Y^T / (k_Y Ap + Z)$. The superscript T indicates total protein concentrations and A^T, as part of the receptor complex, is set to T^T. In above equation we neglected the small contribution of the phosphoacceptor CheB as $k_Y Y^T \gg k'_B B^T$ [9], with k_Y and k'_B the rates of phosphate transfer from CheAp to CheY and CheB, respectively. As Ap and R are linked through Eqs. (3) and (4), a small increase in the amount of methyltransferase, $R + \Delta R$, results in a change of phosphorylated receptors given by

$$\Delta Ap = \left[\alpha + \beta \, \frac{\partial Bp}{\partial Ap} \right]^{-1} \gamma \, \Delta R \tag{5}$$

To arrive at Eq. (5) we have performed a linear expansion around fixed values for the remaining protein concentrations. The linear expansion coefficients α, β can be shown

to have equal sign (see supplement). The derivative $\partial Bp/\partial Ap > 0$ manifests the higher robustness against perturbations of the network topologies Fig. 1c, 1d. This contribution increases the amount of methylesterase, CheBp, whenever the activity of the receptor is rising and thus partially compensates with a stronger methyltransferase. This term is absent in topologies Fig. 1a and 1b, as here CheB is not phophorylated and thus $\partial Bp/\partial Ap = 0$. Fluctuations in protein levels of CheB, CheY and CheZ are compensated for in an equivalent way (see Supplementary Information). Variations in the levels of receptor proteins and CheA are not critical for all topologies. This is because the concentration of CheAp depends only on the number of active receptors which is precisely regulated by the adaptation mechanism [27]. From this perspective it is not surprising to find all cytosolic proteins located on the same operon in order to minimise intrinsic noise (see Fig. 2b) whereas proteins of the receptor-kinase complex are placed on different operons.

Methods

Bacterial strains and plasmids. All strains used in this study were derived from a wild-type chemotaxis strain RP437 using pAMPts homologous recombination system of allele exchange, described before [28]. Strain VS162 carries a *cheY-eyfp* fusion construct in place of a *cheY* gene on the chromosome and strain LL6 carries *cheY-eyfp* and *cheA-ecfp* fusion constructs in place of *cheY* and *cheA* genes on the chromosome. Strains VS102 (*flgM*) and LL1 (*cheY-eyfp flgM*) carry in-frame deletions of an anti-sigma factor FlgM that controls the expression of all chemotaxis and flagellar (class III) genes. Plasmid pLL16 Amp^R encodes FlgM expressed under control of an isopropyl β-D-thiogalactoside (IPTG)-inducible promoter pTrc. Plasmid pVS88 encodes CheY-YFP and CheZ-CFP fusion proteins transcribed as one polycistronic mRNA form pTrc promoter [29]. For the FRET experiments, pVS88 was transformed in VS104 (*cheY cheZ*) or LL4 (*cheY cheZ flgM*) strain and expression was induced by 50μM IPTG. For the co-expression experiments, pVS88 was transformed in RP437 and expression was induced by varying amounts of IPTG. The level of CheY-YFP expression from a native promoter (VS162) was closely matched by the expression in absence of IPTG.

Growth conditions. All strains were grown under standard chemotaxis conditions at 34°C in tryptone broth (TB) as described before [28, 29] in presence of varying amounts of IPTG. Swarm assays were performed at 34°C on TB plates supplemented with 0.3% agar (Applichem) and indicated concentrations of IPTG.

Quantification of gene expression. Expression of fluorescent reporter proteins in individual cells was quantified using flow cytometry on a FACScan (BD Biosciences) equipped with a 488 nm argon laser, or fluorescence imaging on an Axiovert 200 fluorescence microscope equipped with an ORCA AG CCD camera (Hamamatsu). FACScan data were analysed using CellQuestTM Pro 4.0.1 software. Imaging data were analysed using ImageJ software (Wayne Rasband, NIH) to quantify fluorescence of the entire cell. When tested on the same population, both methods gave essentially identical results.

FRET measurements. FRET assay measures intracellular concentration of the

CheYp-CheZ complex as a reporter of kinase activity [12]. CheY and CheZ were expressed as fusions to yellow and cyan fluorescent proteins, YFP and CFP, respectively, and steady-state level of the complex was derived from changes in CFP and YFP fluorescence upon stimulation with a saturating level (100μM) of attractant α-methyl-DL-aspartate. FRET measurements were performed as described before [9, 29] on a Zeiss Axiovert 200 microscope using a 75 Watt super-quiet Xe-lamp (Hamamatsu) for illumination.

Description of the mathematical model. All simulation where performed using *Matlab* from the *The MathWorks* group. For our simulations we assumed a two-state model for the receptor complex as proposed in Ref. [3]. The response of the system to chemo-ligand is described by Michaelis-Menten kinetics, as in Ref. [30]. Response times and amplitudes of CheYp to a sudden change in chemo-ligand are estimated from experiments and determine already the kinetic constants for phosphorylation and dephosphorylation of CheY, assuming an adapted level of one third of the total concentration [4]. The probability of a receptor complex to switch to an active or inactive state for a given methylation level is taken from *in vivo* response measurements to chemo-attractant [9]. The protein concentrations for the individuals of a population are generated from a random process which reproduces the experimentally found gene expression noise shown in Fig. 2. The average concentrations of the chemotaxis proteins are taken from Ref. [7] for the strain RP437 assuming a cell volume of 1.4 fl. To allow for comparison of the different network topologies, we adjust the kinetic parameters of the methylation process to show minimal variation from the optimal response behaviour under the experimentally determined gene expression noise. A detailed description of the mathematical model is given in the Supplementary Information.

[1] Kitano, H. Biological robustness. *Nat. Rev. Gen.* **5**, 826–837 (2004).

[2] Szurmant, H. and Ordal, G. W. Diversity in chemotaxis mechanisms among the bacteria and archaea. *Microbiol. and Mol. Biol. Rev.* **68**, 301–319 (2004).

[3] Barkai, N. and Leibler, S. Robustness in simple biochemical networks. *Nature* **387**, 913–917 (1997).

[4] Alon, U., Surette, M. G., Barkai, N., and Leibler, S. Robustness in bacterial chemotaxis. *Nature* **397**, 168–171 (1999).

[5] von Dassow, G., Meir, E., Munro, E. M., and Ordell, G. M. The segment polarity network is a robust developmental module. *Nature* **406**, 188–191 (2000).

[6] Eldar, A., Dorfman, R., Weiss, D., Ashe, H., Shilo, B. Z., and Barkai, N. Robustness of the BMP morphogen gradient in drosophila embryonic patterning. *Nature* **419**, 304–308 (2002).

[7] Li, M. and Hazelbauer, G. L. Cellular stoichiometry of the components of the chemotaxis signaling complex. *J. Bacteriol.* **186**, 3687–3694 (2004).

[8] Hartwell, L. H., Hopfield, J. J., Leibler, S., and Murray, A. W. From molecular to modular cell biology. *Nature* **402**, 47–52 (1999).

[9] Sourjik, V. and Berg, H. C. Receptor sensitivity in bacterial chemotaxis. *Proc Natl Acad Sci USA* **99**, 123–127 (2002).

[10] Duke, T. A. J. and Bray, D. Heightened sensitivity of a lattice of membrane receptors. *Proc. Natl. Acad. Sci. USA* **96**, 10104–10108 (1999).

[11] Bray, D., Levin, M. D., and Morton-Firth, C. J. Receptor clustering as a cellular mechanism to control sensitivity. *Nature* **393**, 85–88 (1998).

[12] Sourjik, V. Receptor clustering and signal processing in E. coli chemotaxis. *Trends Microbiol.* **12**, 569–576 (2004).

[13] Wadhams, G. H. and Armitage, J. P. Making sense of it all: bacterial chemotaxis. *Nat. Rev. Mol. Cell Biol* **5**, 1024–1037 (2004).

[14] Webre, D. J., Wolanin, P. M., and Stock, J. B. Bacterial chemotaxis. *Curr. Biol.* **13**, 47–49 (2003).

[15] Mello, B. and Yuhai, T. Perfect and near-perfect adaption in a model of bacterial chemotaxis. *Biophys. J.* **84**, 2943–2956 (2003).

[16] Korobkova, E., Emonet, T., Vilar, J. M. G., Shimizu, T. S., and Cluzel, P. From molecular noise to behavioural variability in a single bacterium. *Nature* **428**, 574–578 (2004).

[17] Vaknin, A. and Berg, H. C. Single-cell FRET imaging of phosphatase activity in the Escherichia coli chemotaxis system. *Proc Natl Acad Sci USA* **101**, 17072–17077 (2004).

[18] Elowitz, M. B., Levine, A. J., Sigga, E. D., and Swain, P. S. Stochastic gene expression in a single cell. *Nature* **297**, 1183–1187 (2002).

[19] Kalir, S., McClure, J., Pabbaraju, K., Southward, C., Ronen, M., Leibler, S., Surette, M. G., and Alon, U. Ordering genes in a flagella pathway by analysis of expression kinetics from living bacteria. *Science* **292**, 2080–2083 (2001).

[20] Aldrige, P. and Hughes, K. T. Regulation of flagnellar assembly. *Curr. Opin. Microbiol.* **5**, 160–165 (2002).

[21] Rosenfeld, N., Young, J. W., Alon, U., Swain, P., and Elowiz, M. B. Gene regulation at the single-cell level. *Nature* **307**, 1962–1965 (2005).

[22] Swain, P. S., Elowitz, M. B., and Siggia, E. D. Intrinsic and extrinsic contributions to stochasticity in gene expression. *Proc. Natl. Acad. Sci. U S A* **99**, 12795–12800 (2002).

[23] Swain, P. S. Efficient attenuation of stochasticity in gene expression trough post-transcriptional control. *J. Mol. Biol.* **344**, 965–976 (2004).

[24] Cluzel, P., Surette, M., and Leibler, S. An ultrasensitve bacterial motor revealed by monitoring signaling proteins in single cells. *Science* **287**, 1652–1655 (2000).

[25] Raser, J. M. and O'Shea, E. K. Control of stochasticity in eukaryotic gene expression. *Science* **304**, 1811–1814 (2004).

[26] Sachs, K., Perez, O., Peer, D., Lauffenburger, D. A., and Nolan, G. P. Causal protein-signaling networks derived from multiparameter single-cell data. *Science* **308**, 523–529 (2005).

[27] Yi, T.-M., Huang, Y., Simon, M. I., and Doyle, J. Robust perfect adaption in bacterial chemotaxis through integral feedback control. *Proc. Natl. Acad. Sci. U S A* **97**, 4649–4653 (2000).

[28] Sourjik, V. and Berg, H. C. Localization of components of the chemotaxis machinery of escherichia coli using fluorescent protein fusions. *Mol. Microbiol.* **37**, 740–751 (2000).

[29] Sourjik, V. and Berg, H. C. Functional interactions between receptors in bacterial chemotaxis. *Nature* **428**, 437 (2004).

[30] Rao, C. V., Kirby, J. R., and Arkin, A. P. Design and diversity in bacterial chemotaxis: a

comparative study in E. coli and Bacillus Subtilis. *PLoS Biology* **2**, 239–251 (2004).

Acknowledgments

We thank T. Shimizu, M. D. Levin and K. Lipkow for comments on the manuscript. This work was supported by ZMBH funding and DFG and BMBF grants.

Competing interests statement The authors declare that they have no competing financial interests

Supplementary Information accompanies the paper

Figure 1:

Four possible network topologies of bacterial chemotaxis showing precise adaptation within the experimentally found range of ligand concentrations. Links between proteins indicate activations (arrows) or repressions (bar-ends). Enzymatic reactions are indicated by arrows pointing on lines. The receptor can either be in an active state (red) or inactive state (white). The proteins invoved are denoted by A = CheA, R = CheR, B = CheB, Y = CheY and Z = CheZ, with their corresponding phophorylated forms Ap = CheAp, Bp = CheBp, and Yp = CheYp. The methylesterase (CheB) works only on active receptors which results in an integral feedback control. The response regulator CheY is activated by phosphor-transfer from CheAp. **a**, minimal model as proposed by Barkai & Leibler as explained in the main text. **b**, same as model **a** but with a phosphatase CheZ substituting auto-dephosphorylation of CheYp in topology **a**. **c**, same as model **b** but only the phophorylated form of CheB can build a complex with active receptors. **d**, same as topology **c** with alternative feedback loops drawn as dashed line. The signalling networks **a** and **b** are hypothetical while **c** and **d** represent essentially all known and proposed network topologies for bacterial chemotaxis.

Figure 2:

Gene expression noise of the chemotaxis proteins CheY, CheZ and CheA. **a**, FACS measurements of intercellular variations in the level of CheY, expressed as a YFP fusion from the native chromosomal position. Here, the distribution of wild type cells (red line) is characterised by mean $n = 1$ and the standard deviation $\sigma = 0.67$. For the *flgM* mutant (black line), where the levels of all chemotaxis proteins are upregulated, we have mean $n_F = 6.66$ and standard deviation $\sigma_F = 3.17$. The gene expression noise of the FlgM mutant, $\sigma_F/n_F = 0.47$ is thus smaller as the corresponding value for the wild type, $\sigma/n = 0.67$. Inset: data as in the main panel but normalised to same maximum intensity and with YFP fluorescence displayed on logarithmic scale to illustrate that gene expression noise follows approximately a log-normal distribution. **b**, Correlation of the expression of CheY-YFP and CheZ-CFP from a single pTrc promoter in the absence of IPTG and under control of native ribosome-binding sites. Expression levels were determined using fluorescence imaging as described in Methods; values for intrinsic and extrinsic noise are given by $\eta_{in} = 0.20$ and $\eta_{ex} = 0.44$. Inset: correlation of the expression of CheY-YFP and

CheA-CFP from the native chromosomal positions, determined as in **b**, with $\eta_{in} = 0.26$ and $\eta_{ex} = 0.35$.

Figure 3:

Effect of the total concentration of signalling proteins on chemotaxis. **a**, Chemotaxis efficiency of *flgM* (VS102) cells, expressing varying levels of FlgM from a plasmid. Chemotaxis efficiency was determined in a trypton-broth soft agar (swarm) assay and normalized to that of the wild-type (RP437) cells. Relative mean expression of chemotaxis proteins at each FlgM level was measured as in Fig. 2a, using LL1 strain as a background. Dashed line is a guide to the eye. Note that the detailed evaluation of the relation between chemotaxis and protein expression below the wild-type level is complicated by an adverse affect of the high levels of FlgM on flagella synthesis. Inset: Fraction of chemotactic cells from computer simulations in a population of 10^4 individuals under wild type gene expression noise. Black line: topology Fig. 1c; red line: BL topology Fig. 1a; green line: topology Fig. 1c, but with a phophatase substiting auto-dephosphorylation of CheBp; blue line: topology Fig. 1c, but with CheR binding with Michaelis-Menten constant $K_R = 3\mu$M to the receptor complex; orange line: topology Fig. 1b. **b**, Relative kinase activity in *flgM* cells. Black bar: kinase activity in LL4 cells, experimentally determined in a FRET-based assay. Gray bars: kinase activtiy determined from the mathematical model for differnt network structures. Error bars indicate standard errors.

Figure 4:

Fraction of chemotactic cells as determind by computer simulations for varying strenght of gene expression noise and for differnt network topologies; black line: topology Fig. 1c, red line: BL model Fig. 1a, blue line: topology Fig. 1b, and green line: topology Fig. 1d. **a**, Extrinsic noise varying up to 4-fold the wild type strength and intrinsic noise kept at wild type value, $\eta_{in} = 0.2$. **b**, same as **a** but with varying strength of intrinsic noise and extrinsic noise fixed to the wild type value $\eta_{ex} = 0.44$.

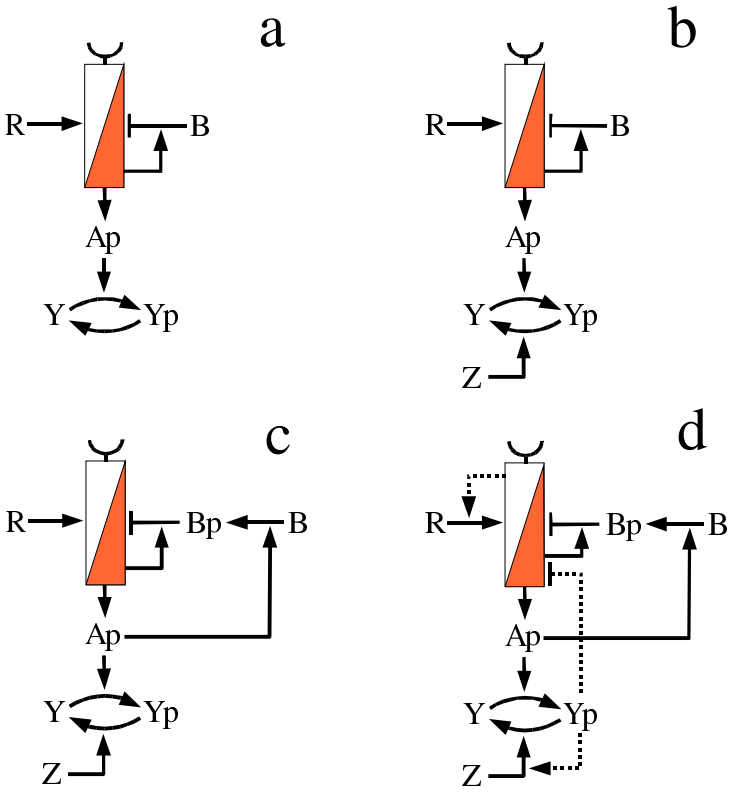

Figure 1

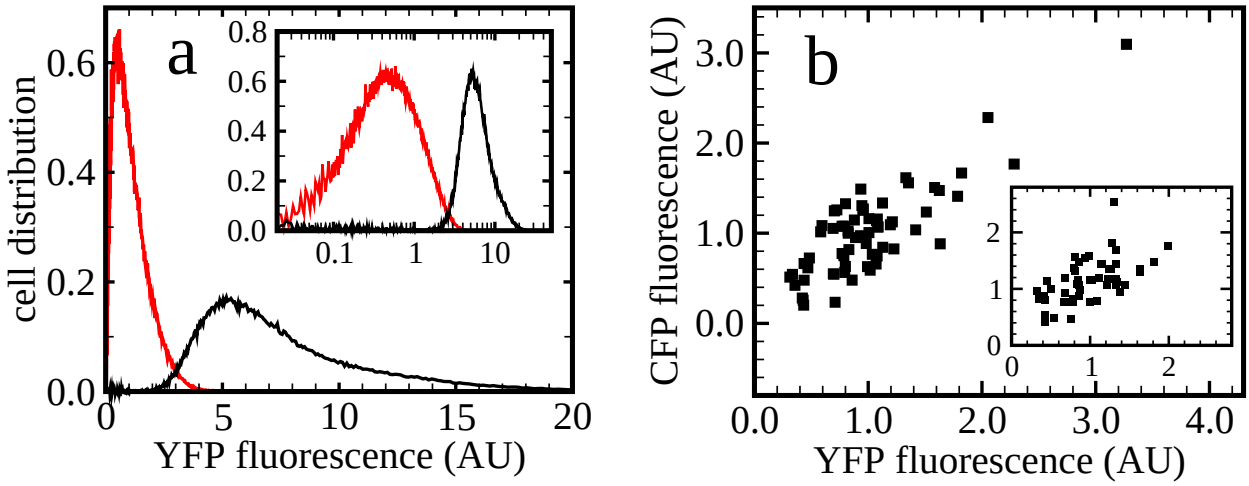
a
cell distribution
YFP fluorescence (AU)
b
CFP fluorescence (AU)
YFP fluorescence (AU)

Figure 2

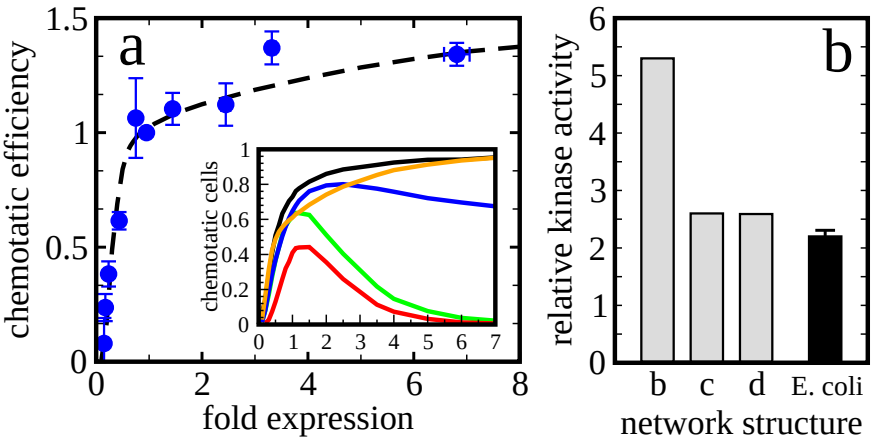
a
b
chemotatic efficiency
fold expression
chemotatic cells
relative kinase activity
network structure
b
c
d
E. coli

Figure 3

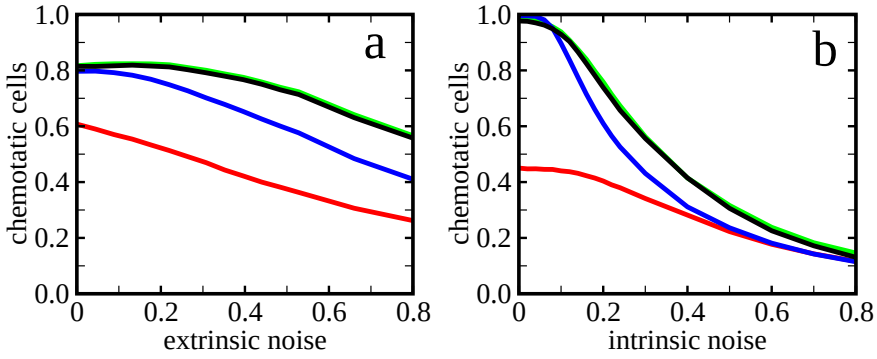
a
b
chemotatic cells
chemotatic cells
1.0
0.8
0.6
0.4
0.2
0.0
0
0.2
0.4
0.6
0.8
extrinsic noise
intrinsic noise

Figure 4